Assessment of the turbulent flow upstream of the Meygen Phase 1A tidal stream turbines

Daniel Coles[1*], Charles Greenwood[2], Arne Vogler[2,3], Tom Walsh[1] and David Taaffe[1]
[1]Simec Atlantis Energy, 4th Floor, Quay 2, 139 Fountainbridge, Edinburgh, UK, EH3 9QG
[2]University of the Highlands and Islands, Lews Castle College, Stornoway, Isle of Lewis, UK, HS2 0XR
[3]Hebrides Marine Services Ltd, Fasgadh, Shawbost, Isle of Lewis, UK, HS2 9BD
[*]E-mail: daniel.coles@simecatlantis.com

***Abstract*—New tidal flow measurements have been obtained upstream of the Meygen Phase 1A turbines from recent bed mounted acoustic doppler current profiler deployments. This paper presents a preliminary assessment of the flow speed and direction, streamwise turbulence intensity and wave climate at two of the turbine locations. Flow speeds and directions are strongly influenced by proximity to Stroma, which diverts the flow into the Inner Sound, resulting in higher speeds and available energy at the north of the site. Comparisons of the average flood and ebb flow directions at each of the turbine locations show differences of 10°. Streamwise turbulence intensities were found to be greatest during ebb tides at the two study locations. Initial results suggest that this is caused by both bed and wave generated turbulence. Large roughness features located to the east (ebb side) of the turbines are the likely cause of eddy shedding and increased shear in the outer flow. Wave measurements show that wave height and zero up crossing period were greatest during ebb tides when wave propagation opposes the flow direction. Preliminary power curve testing shows that the average coefficient of power of the Meygen Phase 1A turbines is 0.41, which exceeds their contractual requirement by 8%. Preliminary results indicate that the turbines are performing well in response to the different turbulent onset flows observed at the Meygen site.**

***Index Terms*—Tidal stream energy, Meygen Phase 1A, streamwise turbulence intensity, bathymetry, waves.**

I. Introduction

In April 2018 Atlantis Resources completed the construction phase of Meygen 1A, the world's largest capacity tidal stream turbine array to date. Meygen 1A is the precursor to the development of 398 MW of installed capacity at the Meygen site, with 86 MW already consented and 252 MW of grid connection agreements in place [1]. Figure 1a-b shows the location of the Meygen site in the Inner Sound between mainland Scotland and the island of Stroma. Figure 1a also shows five additional array allocations in Orkney waters. Four of the arrays are located in the Pentland Firth; Meygen (398 MW [2]), Ness of Duncansby (100 MW [3]), Brough Ness (100 MW [4]) and Brims (200 MW [5]). Westray South (200 MW [6]) and Lashy Sound (10 MW [7]) are located north of the Pentland Firth, to the west and east of Eday respectively. The total array capacity allocation of the six arrays exceeds 1 GW, with 6 MW of capacity installed to date (all at Meygen). Figure 1a also shows the Fall of Warness to the south-west of Eday, which is the location of the European Marine Energy Centre (EMEC) [8].

The Meygen Phase 1A array utilises two different turbine technologies; three Andritz Hydro Hammerfest turbines (referred to as T1-3 from now on) and one Atlantis AR1500 turbine (referred to as T4 from now on). All four turbines have a power rating of 1.5 MW, giving a total array capacity of 6 MW. Each turbine is installed on a gravity-based turbine support structure, each weighting between 250 and 350 tonnes, coupled with 6 ballast blocks weighing 1,200 tonnes to provide horizontal stability. Each turbine has a dedicated sub-sea cable laid directly on the seabed that is brought ashore via a horizontal directionally drilled borehole within the foreshore bedrock. The cables connect the turbines to an onshore power conversion unit building at the Ness of Quoys, where power converters and transformers make the power grid code compliant prior to export into the local distribution network.

Figure 1b-c shows the location of the four Phase 1A turbines at Meygen. The location of four bed mounted Acoustic Doppler Current Profilers (ADCP) are also shown. The bed mounted ADCPs were deployed between August and December 2017 in order to characterise the onset flow conditions to each of the turbines during either the flood or ebb tides.

This paper presents a preliminary analysis of the newly obtained bed mounted ADCP data. This includes an assessment of flow speeds and directions, boundary layer profile, streamwise turbulence intensity and wave climate upstream of the turbines. Results presented here build on an analysis of historic ADCP data obtained within the Inner Sound in 2015 at a single location (58.6595°N, 3.1411°W) [10], which found:

1) The flow exhibited significantly different properties depending on flow direction, with greater turbulence intensities during ebb tides.
2) Largest turbulent length scales were observed at high flow speeds. Length scales between 50-60 m were measured at flow speeds above 2.5 m/s.
3) When waves and tide are in the same direction, turbulent fluctuations were dominated by orbital motion.
4) When wave and tidal directions are opposed, the turbulence appeared to be more random.

The novelty of the work presented in this paper lies in our analysis of the spatial variability in the onset turbulent flow to the Meygen Phase 1A turbines, by comparing flow features at two locations. To our knowledge, this is the first work that

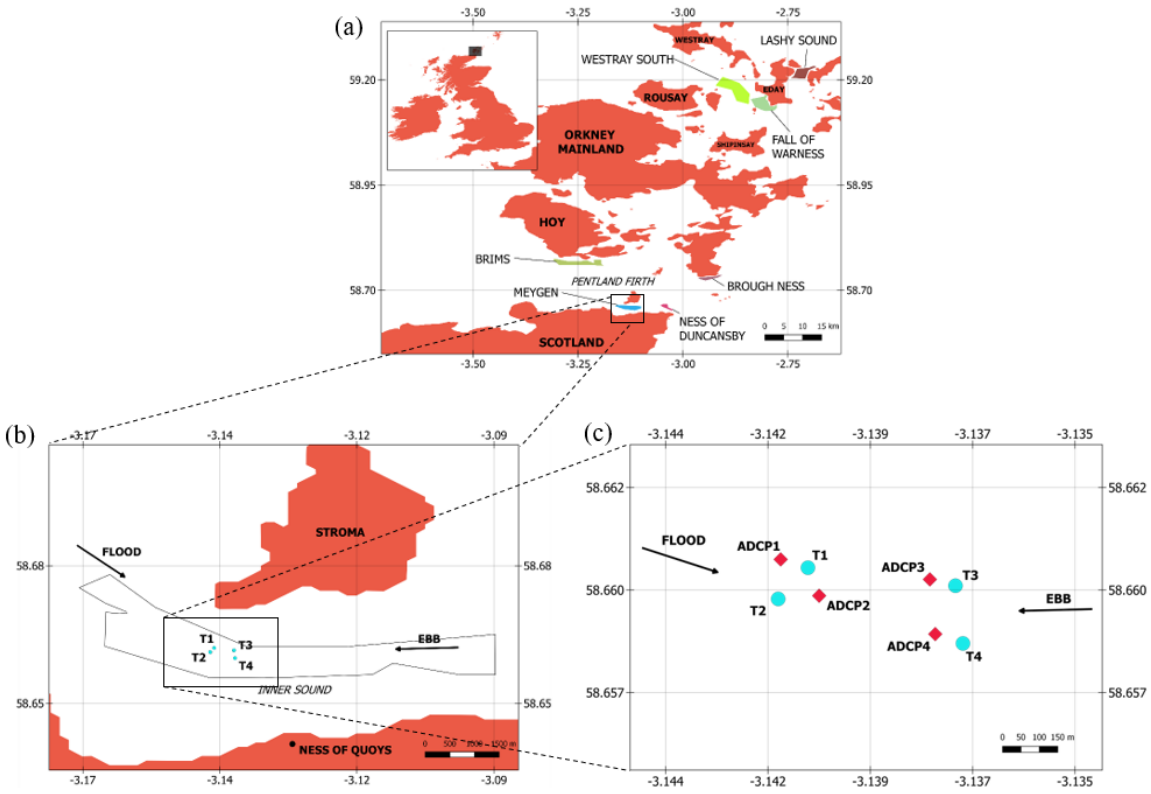

Fig. 1. (a) The locations of seven development plots with a total capacity of over 1.05 GW in Orkney waters (b) Meygen Phase 1A array, located in the Inner Sound between mainland Scotland and the Island of Stroma in the Pentland Firth, Scotland. The location of the four Phase 1A turbines are shown by black points, and the locations of four bed mounted ADCP's are shown by red diamonds. The direction of flood and ebb tides is also shown. (c) Layout of Meygen Phase 1A turbines (T1-4) and bed mounted ADCPs (ADCP1-4).

presents flow data from multiple locations in the presence of a multi-MW array of tidal stream turbines.

II. Meygen Field Measurements

In late 2017 bed mounted ADCPs were deployed at each of the Meygen Phase 1A turbines. The locations of the ADCPs are shown in Figure 1b-c. An analysis of high resolution bathymetry data was conducted to identify suitable locations for the ADCP deployments, ensuring undesirable irregularities on the seabed were avoided. Remotely Operated Vehicle (ROV) support was used to check the sea bed conditions prior to siting the ADCPs, and also to check the ADCP frames were sitting in a stable position before the deployment cable was disconnected, also using the ROV. Locational accuracy was achieved using an Ultra-Short Baseline (USBL) communication system on the deployment line to provide heading and distance between ADCP and a Differential-GPS on the surface vessel via an acoustic modem. The ROV was also used for the ADCP frame recovery by hooking the recovery cable into dedicated ROV handles mounted onto the frames.

The ADCPs were located approximately two rotor diameters upstream of T1, T3 and T4 on the flood tide and at a similar distance upstream of T2 on the ebb tide. This distance between ADCPs and turbines was chosen in order to prevent the turbine influencing the flow measurements, whilst also ensuring the ADCPs were close enough to the turbines to capture flow that is representative of the un-impinged flow at the location of the turbine, in accordance with IEC 62600-200 [15]. The primary purpose of the ADCP deployments was to characterise the onset flow conditions to each of the turbines in order to conduct Power Curve Tests (PCT).

Two different ADCPs were used during the campaigns; a Nortek Signature 500 and a Teledyne RDI V50. Table I summarises the technical specification of the two ADCPs. Both units feature five beams, one vertically aligned to monitor the vertical velocity profile and also to allow for tracking of the sea surface for wave measurement. The other four beams are slanted at 25° from the vertical axis and are aligned at 90° between beams covering the full 360° circle. The acoustic frequency of 500 kHz was suitable for the water depth around 30 m and units were set up to ping with all 5 beams at a 2 Hz frequency over bin sizes of 1 m. The specification for both units is very similar, and key differences are the improved ability of the Signature 500 to capture wave data by pulsing a dedicated wave burst from the vertical beam with a modified bin size to allow detection of a higher level of detail of the sea surface displacement. Both ADCPs store the raw beam data for all bursts, together with additional information on pitch, roll, compass heading, pressure and temperature. For the purpose of this study the raw beam velocity datasets were post-processed

using Matlab to convert from beam co-ordinates to streamwise, east, north and upwards velocities. This included compensation for pitch and roll where this occurred.

TABLE I
TECHNICAL SPECIFICATION OF THE NORTEK SIGNATURE 500 AND TELEDYNE SENTINEL V20 ACOUSTIC DOPPLER CURRENT PROFILERS.

	Nortek Signature 500	**Teledyne Sentinel V50**
Sampling freq.	2 Hz	2 Hz
Burst interval	Continuous	Continuous
No. beams	5	5
Beam angle	25°	25°
Bin size	1 m	1 m
Number of bins	44	39
Blanking dist.	0.5 m	1 m
Velocity res.	0.1 m/s	0.1 m/s
Min. accuracy	0.3% of measured value	0.3% of measured value

TABLE II
SUMMARY OF ADCP DEPLOYMENTS.

	ADCP	**Flood/ebb side**	**Data capture period**
T1	Nortek Signature	Flood	15/10/17 — 12/12/17
T2	Teledyne Sentinel	Ebb	3/8/17 — 30/8/17
T3	Nortek Signature	Flood	3/8/17 — 30/8/17
T4	Teledyne Sentinel	Flood	15/10/17 — 12/12/17

The ADCP compasses were calibrated following manufacturer's guidelines to avoid magnetic directional errors of the measured data. This involved the use of a dedicated ADCP stand to allow rotation of the ADCP under varying vertical angles in case of the V50. The compass of the Signature 500 was calibrated with the unit fitted inside the frame and suspended from a non-magnetic structure whilst rotating it around its axis. The magnetic variation at the site during the deployments was 3.3°W, and this value was subtracted from the compass heading to convert the raw heading data to true north. Only non-magnetic materials were used for the deployment frames. A maximum distance was maintained between the battery packs and ADCPs to avoid any magnetic interference.

Two different types of ADCP frames were used for the deployments. A computer aided design of the first frame is shown in Figure 2. The frame has a square base and houses the Teledyne V50. The frame includes vortex generators to minimise drag forces and turbulence within the sensor chamber [1]. Figure 3 shows a photograph of the second frame on the seabed, housing the Nortek Signature 500. Both frames have a dry mass of around 400 kg and footprints of around 2.5 x 2.5 m. Each frame was fitted with a gimbal mount to allow for adjustment of a non-level seafloor and good results were achieved with a damped design developed by the University of Edinburgh under the Redapt project [16].

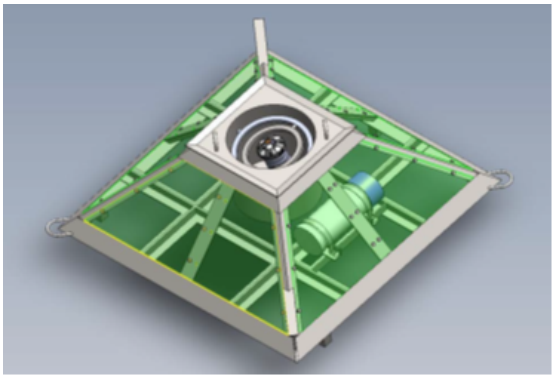

Fig. 2. Illustration of the Acoustic Doppler Current Profiler within its square based supporting frame with battery pack.

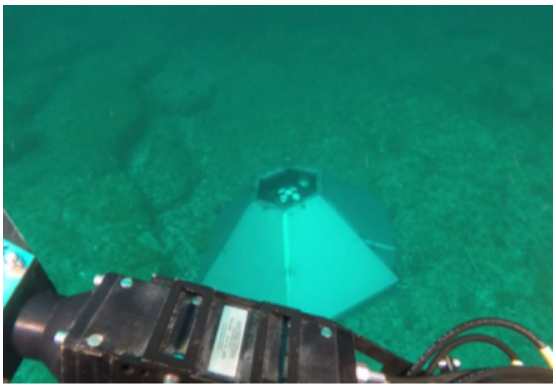

Fig. 3. Photograph of the Nortek ADCP within its hexagonal based support frame on the seabed, obtained from Remotely Operated Vehicle (ROV) footage.

The majority of the results presented in this paper focus on comparisons between the flow characteristics at T2 and T3. The T2 and T3 bed mounted ADCP data sets were obtained over the same data capture period between 3/8/2017 and 20/8/2017. This allowed the flows at T2 and T3 to be compared directly, with full accountability for weather and the time in the spring neap cycle, two features that impact upon the turbulent flow.

In addition to the four bed mounted ADCPs, each turbine has an ADCP located on its nacelle to measure the flow above the top tip blade height. Measurements from the nacelle mounted ADCPs were used to compare the flow occurrence at the location of each turbine during the same data capture period, which was not possible from the bed mounted ADCP measurements. The turbine mounted ADCPs are Teledyne Workhorses. They are powered by the turbine, allowing continuous flow measurements to be obtained through the turbine Supervisory Control And Data Acquisition (SCADA) systems.

III. DATA PROCESSING

Raw beam velocities were converted to streamwise, lateral and vertical components using the approach outlined in [17], where the streamwise axis is aligned with the turbine axis. The 2 Hz ADCP data was averaged over three minute periods to

obtain mean flow speeds. The streamwise turbulence intensity was calculated using Equation 1;

$$I = u'/u \tag{1}$$

Where I is the streamwise turbulence intensity, u' is the root mean square of the turbulent fluctuations and u is the mean flow speed, averaged over three minutes.

In general the ADCPs were stable throughout the deployment periods, with only small variations in ADCP pitch, roll and heading. The signal intensity, correlation and amplitude were also satisfactory throughout the deployment periods. For these reasons no data was excluded from the datasets during the analysis.

IV. Observations from Field Measurements

A. Flow occurrence

Figure 4 shows the flow occurrence at the four turbine locations. Flow speeds were obtained over a three day period falling between spring tide and the following neap. Measurements were obtained using the nacelle mounted ADCPs on each turbine to enable the same data capture period to be used for each of the four turbines. The nacelle mounted ADCPs measure the flow speeds above the Top Blade Tip Height (TBTH), so the flow speed measurements are not representative of the flow speeds incident on the turbine rotor lower in the water column. No corrections were made to account for the boundary layer profile that exhibits lower flow speeds at the turbine hub height than above the turbine. No correction was made to account for flow acceleration above the turbine that occurs as a result of turbine blockage either. It is assumed that the influence of blockage on the flow speed is the same at each turbine location, allowing the analysis to provide an initial comparison of the magnitude of flow speeds experienced at each turbine over the same data capture period.

Results in Figure 4 show that the highest flow speeds are located at the north of the site, at the locations of T1 and T3. Maximum flow speeds during the capture period at T1 and T3 are 4.38 m/s and 4.66 m/s respectively. T2 and T4 are located at the south of the site, where flow speeds are slightly lower. T2 and T4 experienced maximum flow speeds of 4.17 m/s and 4.16 m/s respectively over the same data capture period. Maximum and mean flow speeds are summarised in Table III.

Table III also shows the percentage of time that the flow speed exceeds 3 m/s at each turbine location above the TBTH. At T1 and T3 the flow above the TBTH spends approximately 22% and 23% of the time above 3 m/s respectively. For comparison, at T2 and T4 the flow above the TBTH spends approximately 18% and 16% of the time above 3 m/s respectively.

The Meygen Phase 1A turbines have a rated speed of 3 m/s. At flow speeds greater than 3 m/s, the turbines use blade pitch control in order to maintain a rated power of 1.5 MW. In reality the turbines spent less time at rated power during the chosen capture period than the figures presented in Table III, because the onset flow speed to the turbine over the swept area is less than the flow above the TBTH.

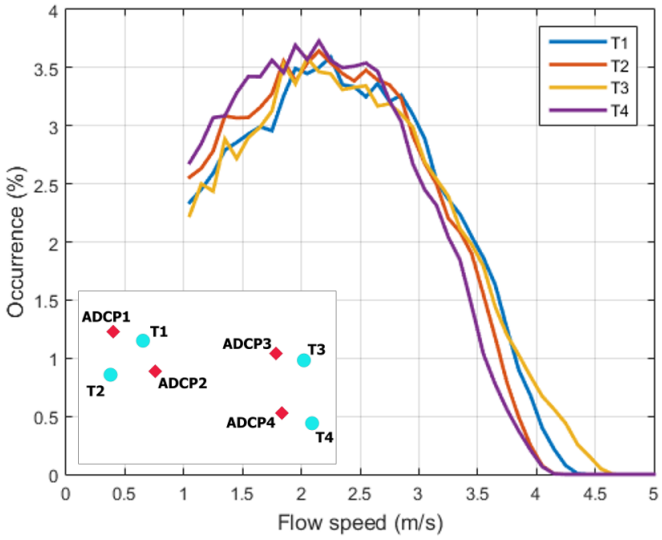

Fig. 4. Flow occurrence at the Phase 1A turbine locations, obtained from ADCPs. Inset shows the location of T1-4 and ADCP1-4.

TABLE III
Summary of maximum and mean hub-height flow speeds above the top tip blade height at T1-4, and the percentage of time the flow exceeds 3 m/s.

Location	Max. flow speed	Mean flow speed	% time over 3m/s
T1	4.38 m/s	2.08 m/s	22.2%
T2	4.17 m/s	2.00 m/s	18.6%
T3	4.66 m/s	2.12 m/s	23.1%
T4	4.16 m/s	1.94 m/s	15.8%

B. Flow direction

Figure 5 displays T2 and T3's tidal rose, showing the hub height flow direction and speed over a common three day period falling between spring tide and the following neap. At T2 the average flood and ebb directions are approximately 122° and 272° relative to north respectively. Most of the scatter in the direction data was observed at slack tide below 1 m/s, which is the cut in speed of the turbines. At T3 the average flood and ebb directions are approximately 133° and 284° respectively. The difference between T2 and T3 average flood direction is 11° and the difference between T2 and T3 average flood direction is 12°.

During flood tides the flow enters the Pentland Firth from the west in a west-east direction (approximately 90° relative to north). The west coast of Stroma is aligned perpendicular to the flow direction upstream of the island, with a span of approximately 3.5 km. Stroma's west coast creates a significant blockage to the incoming flow that diverts the flow by around 43° as it enters the Inner Sound (from 90° upstream of Stroma to 133° at T3). Flow diversion at T2 is less pronounced than at T3. This is likely to be because T2 is further away from Stroma than T3.

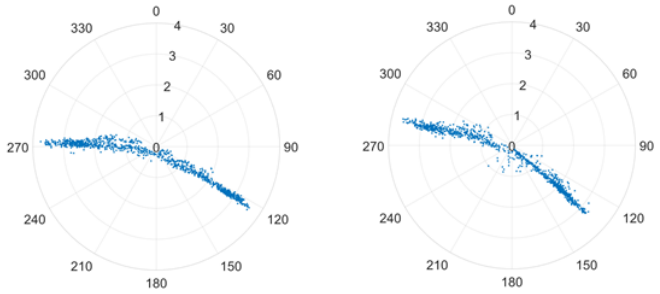

Fig. 5. Tidal rose showing hub height flow speeds (m/s) and directions (degrees relative to north) at T2 (left) and T3 (right). Data is time averaged over three minute periods.

During ebb tides the flow enters the Pentland Firth from the east in an east-west direction (approx. 270° relative to north). Stroma's east coast is also aligned approximately perpendicular to the upstream flow but only spans around 1.7 km. Stroma is more streamlined to the flow during ebb tides in comparison to flood. For this reason the difference between the bulk flow direction upstream of Stroma and the flow direction at the turbines are less pronounced during ebb tides.

Table IV summarises the mean ebb and flood flow directions at hub height, and the variance in the flow direction at hub height at each of the turbine locations. In both cases, flood tides provide a lower directional variance than the ebb tide. This suggests greater directional velocity fluctuations during the ebb tides, which is likely to be as a result of higher turbulence during ebb tides, as discussed later in section IV-*E*.

TABLE IV
SUMMARY OF MEAN HUB-HEIGHT FLOW DIRECTION AND VARIANCE IN FLOW DIRECTION AT HUB HEIGHT AT T2 AND T3 DURING EBB AND FLOOD TIDES.

Location	**Mean hub height direction**		**Variance at *u*=4 m/s**	
	Ebb	Flood	Ebb	Flood
T2	272°	122°	40°	18°
T3	284°	133°	25°	23°

After the turbines were installed the turbine yaw angles were modified to align the turbines with the oncoming flow. This is essential for maximising energy yield. When the flow is misaligned with the turbine axis, the streamwise flow component (i.e. the flow component that is aligned with the turbine axis) is equal to the cosine of the flow magnitude so that turbine power is given by;

$$P = \frac{1}{2}\rho C_p A(Ucos\theta)^3 \quad (2)$$

Figure 6 illustrates the relationship between the angle of the onset flow and the power generated by a tidal stream turbine. Power measurements are normalised by the power generated when the flow is aligned with the turbine axis (i.e. θ=0).

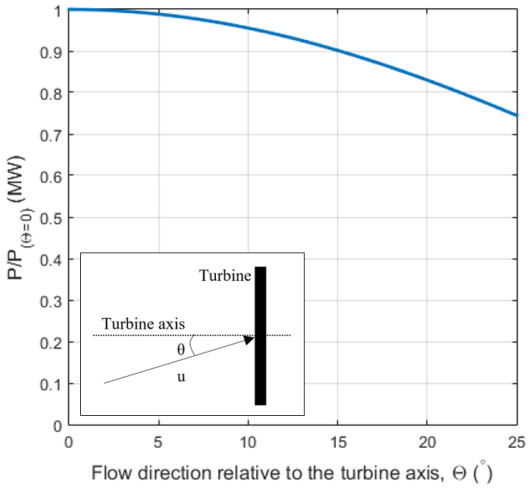

Fig. 6. Relationship between the flow direction relative to the turbine axis and generated power.

Results from a 2D Advanced CIRCulation model (ADCIRC) with 15 minute temporal resolution and 150 m spatial resolution have shown that the mean tidal heading can shift over long time periods [18]. Flow directions extracted from the model at a location in the centre of the Meygen Phase 1A array (at coordinates 58.6577°, 3.1272°) show a shift in the flood heading of 10° from approximately 303° prior to 28th March, to around 293° thereafter. Based on Equation 2, this would lead to a drop in yield of approximately 5% if the yaw angle of a turbine at the same location was not modified to account for the change in flow direction. Work is ongoing to monitor the flow direction using the nacelle mounted ADCPs to modify turbine yaw angles when needed in order to maximise power generation.

C. Flow twist

Figure 7 shows the variation in direction of the streamwise velocity at T2 and T3 through the water column. The subplots on the left show the temporal variation of the mean flows directional deviation with depth. In ebb, the flow angle is greatest (i.e. closest to north) at the bottom of the water column, and gradually reduces (i.e. away from north in the anti-clockwise direction) with proximity to the sea bed. In the flood direction the flow angle is lowest (i.e. closest to north) near to the bed, and gradually increases (i.e. away from north in a clockwise direction) with proximity to the free surfaces. This highlights an oscillating flow twist with the flood and the ebb tide at T2 and T3. In this work we define the flow twist as the difference in flow angle between Bottom Blade Tip Height (BBTH) and Top Blade Tip Height (TBTH). Initial results indicate that twist is typically 5-8° at T2 and T3, but highest at T2 during ebb tides.

In Figure 7 the right-hand plots show the profiles of the mean directional deviation during peak flood (blue) and ebb

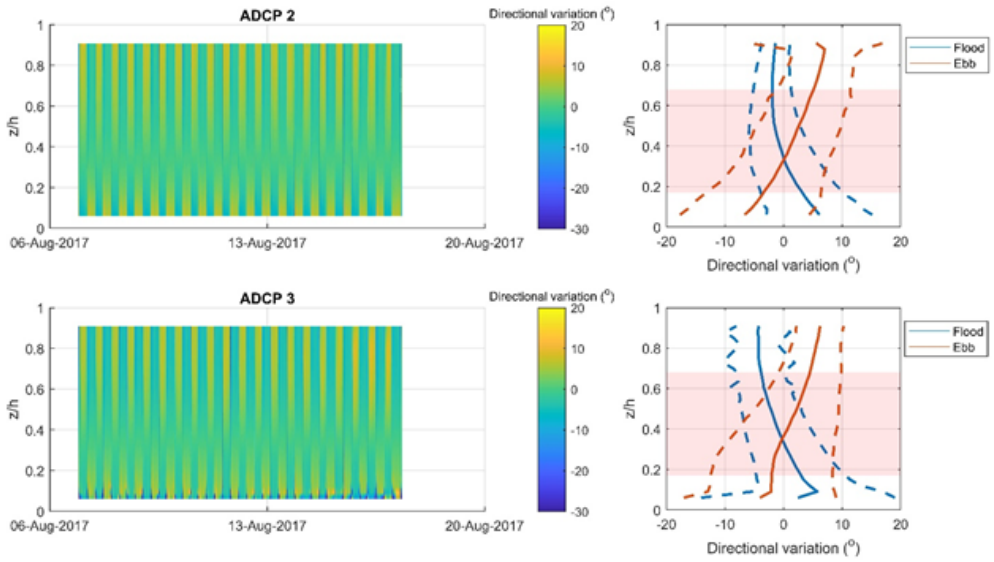

Fig. 7. Temporal variation in flow direction throughout the water column at ADCP 2 and ADCP 3 (left), and the mean peak directional variation in flow direction (right).

(red) tides. The dashed lines indicate the positive and negative standard deviation for the directional variance. This shows a maximum variation at the seabed of 6° for the flood and ebb tide for ADCP 2. Towards the surface, the ebb tide switches from a negative deviation to a positive deviation of -6.5°. This same process occurs for the flood tide on a lesser scale. The standard deviation of the flow profiles shows in all cases a wider spread towards the sea-bed than that of the surface. This is likely to be linked to increased turbulence measured at the bottom of the water column due to bed generated turbulence.

The flow twist has been observed to change during flood tides. At times after low water slack (i.e. at the start of the flood tide) a shallow reef located off Stroma's headland is exposed. As time progresses during the flood tide the reef become submerged. When the reef is exposed at the start of the flood tide all of the flow is diverted around it. As time progresses the reef becomes submerged, allowing some of the flow to pass over the top of the reef, which modifies its direction in the top of two water column compared to earlier in the same tide. Similarly at times after high water slack (i.e. at the start of the ebb tide) the reef is submerged, allowing flow over it. After time the reef becomes exposed, so that the flow at the top of the water column must divert around it.

D. Boundary layer profile

Figure 8 shows characteristic time averaged flow speed profiles at T2 during flood and ebb tides. Three comparisons between ebb and flood profiles are shown, which were selected based on the flow speed at hub height. The low flow speed case compares ebb and flood profiles with hub height flow speeds between 1.0 - 1.1 m/s, where 1 m/s is the cut in speed of the turbines. The second flow case uses profiles with a hub height flow speed between 2.0 - 2.1 m/s. The third flow case uses profiles with a hub height flow speed between 3.0-3.1 m/s (note 3 m/s is the rated speed of the turbines).

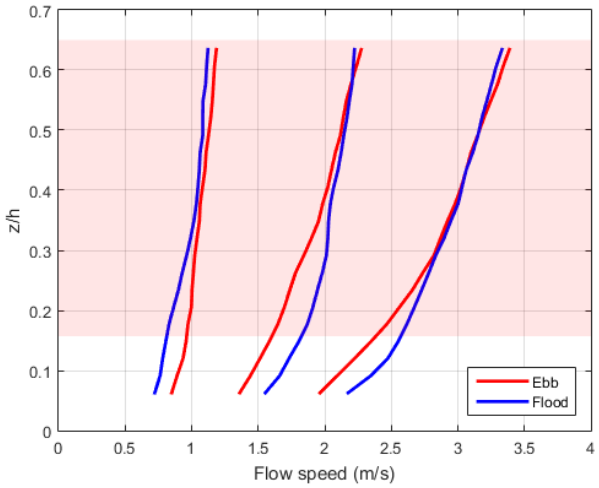

Fig. 8. Comparison between characteristic onset flow speed profiles to T2 during ebb and flood tides. The region taken up by the turbine swept area is shaded pink.

The wake impingement on the location of ADCP2 during flood tides was minimised by using data from a period when T2 was in idle. Regardless of this, T2's wake is unlikely to impinge on the location of ADCP2 because the flood flow angle is approximately 120° relative to north, so ADCP2's location is not aligned with the flood flow and T2's location. The pink shaded region of the graph shows the area taken up by T2's swept area within the water column, where the Bottom Blade Tip Height (BBTH) is z/h=0.16, the Top Blade Tip Height (TBTH) is z/h=0.67, z is the distance above the

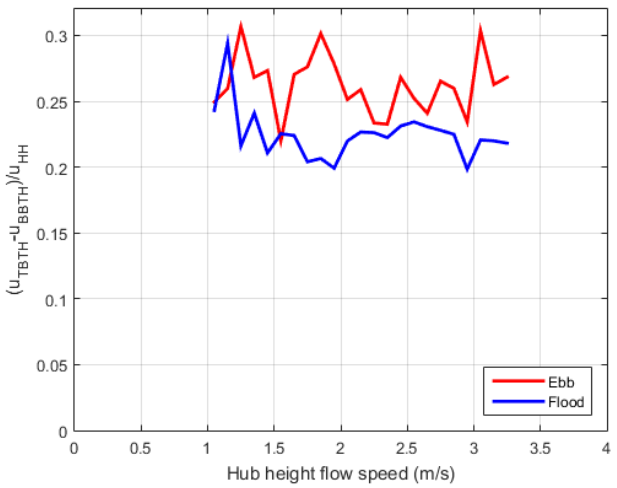

Fig. 9. Difference in flow speed between the Top Blade Tip Height (TBTH) and Bottom Blade Tip Height (BBTH) over Hub Height (HH) during ebb and flood tides at T2. Results are normalised by the hub height flow speed.

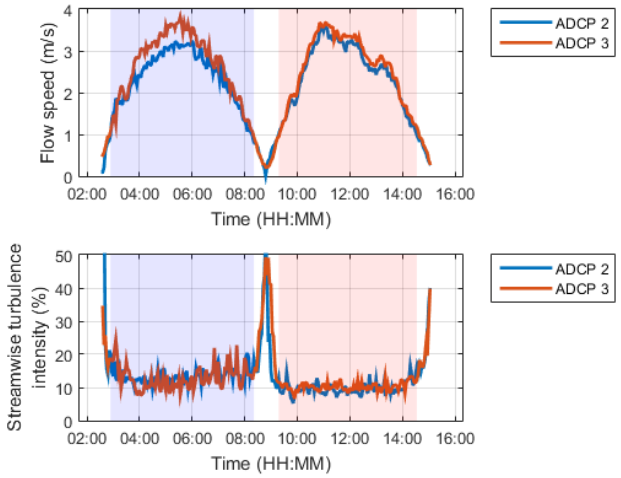

Fig. 10. Flow speed (above) and streamwise turbulence intensity (below) at T2 and T3. The blue shaded region covers the ebb tide, the pink shaded region covers the flood tide.

sea bed and h is the water depth at Lowest Astronomical Tide (LAT).

The difference in flow speed between TBTH and BBTH over a full range of hub height flow speeds is shown in Figure 9. The time averaged flow profiles were binned based on the hub height flow speed. For the profiles within each bin, the difference in flow speed between the TBTH and BBTH was quantified. The difference was then normalised by the hub height flow speed. Finally the normalised flow speed differences within each bin were averaged.

Results show that T2 experiences the greatest variation in flow speed between TBTH and BBTH during ebb tides over the majority of flow speeds above the turbine cut in speed of 1 m/s. This will be discussed in relation to turbulence generation in section V.

The forces exerted on the turbine blades are proportional to the flow speed squared. Turbine blades are subject to cyclic loading as a result of the difference in the force exerted on them as they rotate, where faster flows at the TBTH exert larger forces than the slower flows at the BBTH. Results indicate that cyclic loading on T2's blades is likely to be lower during flood tides as a result of smaller differences in flow speed between TBTH and BBTH.

E. Turbulence

1) Streamwise turbulence intensity: Figure 10 shows the hub height flow speed and hub height streamwise turbulence intensity at T2 and T3 over an ebb-flood tide. Regions shaded blue cover ebb tide periods when flow speed exceeds the cut in speed of the turbine, which is 1 m/s. Regions shaded pink cover flood tide periods, also when flow speeds exceed the cut in speed of the turbine.

The turbines operates outsie of the streamwise turbulence intensity spikes that occur at low flow speeds below the cut in speed of the turbines. The hub height streamwise turbulence intensity is noticeably higher during ebb tides at T2 and T3. At T2 the mean streamwise turbulence intensity is around 12% during ebb tides at peak flow speed and 10% during the flood. Similarly at T3 the mean streamwise turbulence intensity is approximately 12% during peak ebb tides and 10% during peak flood tides. This finding is in line with turbulence intensity results presented in [10], which also found higher levels of turbulence intensity during ebb tides vs. flood tides from a bed mounted ADCP campaign at coordinates (58.6595°N, 3.1411°W). This location is in close proximity to ADCP 2 and ADCP 3.

Table V summarises streamwise turbulence intensity results obtained at T2-3, alongside field measurements at other sites around the world.

TABLE V
SUMMARY OF STREAMWISE TURBULENCE INTENSITY AT PEAK FLOW AT T2-3, WITH COMPARISONS AT OTHER TIDAL SITES AROUND THE WORLD.

Location	**Streamwise turbulence intensity at peak flow**
Europe	
Meygen, Scotland, T2 (z/h=0.45)	0.12 (ebb), 0.10 (flood)
Meygen, Scotland, T3 (z/h=0.45)	0.12 (ebb), 0.10 (flood)
Strangford Lough, NI (z/h=0.5)	0.05–0.06 (ebb and flood) [12]
Japan	
Kobe Strait, NAG. (z/h=0.5)	0.12–0.15 (flood), 0.12—0.14 (ebb) [19]
Tanoura Strait, NAG. (z/h=0.5)	0.1–0.2 (flood), 0.1—0.2 (ebb) [19]
Naru Strait, NAG. (z/h=0.5)	0.25-–0.35 (flood), 0.1—0.2 (ebb) [19]
America	
East River, NY (z/h=0.5)	0.13 (flood), 0.18 (ebb) [12]
Nodule Point, Wash (z/h=0.2)	0.08—0.11 [13]
Admiralty Head, Wash (z/h=0.14)	0.09–0.12 [13]

In general the levels of mid-depth streamwise turbulence intensity at Meygen are similar in magnitude to those measured

at Kobe Strait in Nagasaki, Japan [19] and the East River in New York, USA [12]. Streamwise turbulence intensity at other sites such as Nodule Point and Admiralty Head in Washington, USA [13] are also similar in magnitude to Meygen, however measurements were taken closer to the seabed.

Measurements at Tanoura Strait and Naru Strait in Japan show higher turbulence intensities at peak flow than at Meygen. One contributing factor to this is likely to be that the peak flow speeds in the straits are lower than at Meygen.

Naru Strait in Japan and the East River in the USA also experience significant differences in turbulence intensity depending on flow direction.

V. Discussion

Results in this paper provide a preliminary assessment of the spatial and temporal variations in flow and turbulence at the Meygen site, with a focus on the onset conditions to T2 and T3. In this section we discuss the potential sources of turbulence at the Meygen site in order to better understand the temporal differences (i.e ebb vs. flood) and spatial differences (i.e T2 vs. T3 location). Preliminary turbine performance results are also discussed.

A. Bed generated turbulence

Figure 11 shows the spatial variation in depth within the Inner Sound, with the locations of T1-4 and the directions of the ebb and flood tides also shown. Trench-like features are orientated approximately parallel and perpendicular to the flow directions. The trenches create a 'crosshatch' bathymetric pattern around the turbines. The trenches are up to 6 m deep and vary significantly in width.

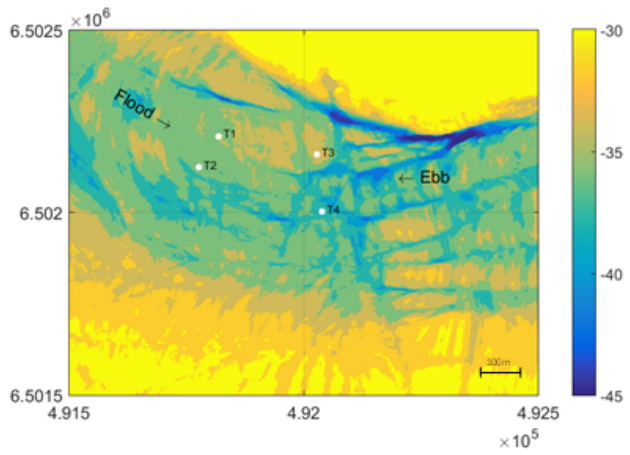

Fig. 11. Spatial variation in depth over the Inner Sound. The locations of T1-4 and the direction of the ebb and flood tides are also shown.

Figure 12 shows the variation in depth in the fetch directly upstream of ADCP2 and ADCP3 during ebb (left) and flood (right) tides. The approach to ADCP2 and ADCP3 appear significantly more rough during ebb tides in comparison to flood. On the ebb side of ADCP2 there is a 6 m deep trench 200 m upstream, orientated perpendicular to the flow direction. The bathymetry levels out between the trench and ADCP2 to a mean depth of approximately 34 m. Smaller scale roughness features are also noticeable over the bed. There is a similar trench located approximately 100 m upstream of ADCP3 on its ebb side, with additional large roughness features exhibiting abrupt reductions in depth further downstream.

In comparison, the bathymetry on the flood side of ADCP2 and ADCP3 shows far smaller roughness features. On the flood side of ADCP2 the depth gradually undulates between approximately 33-37 m. On the flood side of ADCP3 the depth gradually falls away with distance from the ADCP. As with the ebb side, smaller scale roughness features are also noticeable on the flood side of ADCP2 and ADCP3.

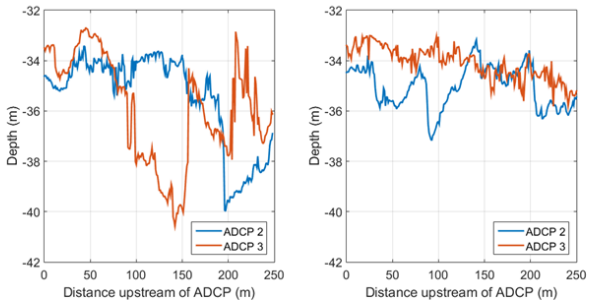

Fig. 12. Variation in depth over a 200 m fetch upstream of ADCP2 and ADCP3 on ebb (left) and flood (right) tides.

Trench-like roughness features orientated perpendicular to the flow can enhance turbulence within the outer flow. This occurs when eddies are shed off the trailing edge of the trenches, as illustrated in Figure 13. These eddies augment shear, which generates turbulence. Results in section IV-*D* (Figure 8 and 9) imply higher levels of shear in the boundary layer during ebb tides than during flood tides at T2. As a result the turbulence generated by shear is also likely to be higher during ebb tides than flood tides at T2.

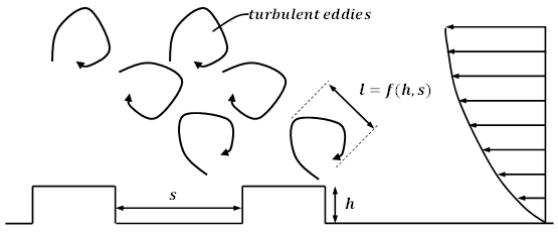

Fig. 13. Illustration of eddies shed off leading edge of trench-like bed roughness features.

The pitch ratio describes the ratio between the roughness height (h in Figure 13) and the trench fetch (s in Figure 13). For a pitch ratio less than 4 (known as d-type roughness), eddy separation is confined to the trenches so that the bulk flow 'rides' over the roughness elements, minimising the influence of eddy shedding by the trenches on the turbulence in the outer flow [20]. For a pitch ratio greater than 4 (known as k-type roughness) separation and reattachment occurs between

roughness elements, causing larger eddies to shed off the leading edge of the roughness elements and emanate into the outer flow, enhancing ambient turbulence intensities [21]. Large Eddy Simulations (LES) of flow over trenches orientated perpendicular to the flow has shown that k-type roughness with a pitch ratio of 10 has the greatest impact on augmenting turbulence intensities in the outer flow [20]. Based on these findings, the higher level of roughness on the ebb side of ADCP 2 and ADCP 3 is a likely contributing factor to the higher levels of turbulence that have been observed during ebb tides.

B. Waves

Figure 14 shows timeseries plots of the spectral moment derived wave height and zero up crossing period during August 2017 at T2 and T3, and November at T4. A summary of wave height and zero up crossing period (mean and range) during these periods is shown in Table VI.

During the deployments no large storm events occurred. However, there are several instances where wave height exceeded 3.5 meters during the winter ADCP deployment at T4, as shown in Figure 14. These higher wave heights are likely to increase the level of onset turbulence to T1-4 during the winter months, as a result of wave induced orbital motion.

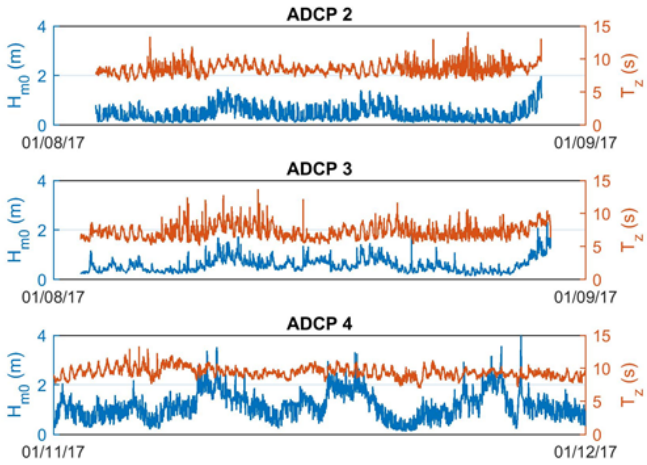

Fig. 14. Wave height and zero up-crossing period for 4 deployments from each of the ADCP locations.

Even during the calmer sea states in August the effects of wave induced turbulence throughout the water column is highly likely. This can be assumed if the dispersion relation is considered and the wavelength is calculated [22]. For example, a wave with a period of 10 s in 33 m water depth would produce a wavelength of 140.5 m. Wave particle velocities are shown to propagate to depths of half their wavelengths. Ensuring that for this case, it is very likely that this surface wave would result in significant turbulence interference at turbine depths.

When the wave height and period are separated into the flood and ebb tidal phases the effect of the tide can be seen on the mean and range for the wave parameters (Table VI). The prevailing wave direction for the site is aligned with the flood tide direction, as a result of the exposure of the site to the Atlantic Ocean. This means that for most cases waves will propagate with the flood tide, and oppose the ebb tide. The difference in measured wave parameters shows smaller mean values of both wave height and zero up crossing period during the flood tide.

C. Turbine performance

A preliminary turbine performance assessment has been conducted in order to correlate the onset turbulent flow conditions to the generated power of each of the four Meygen turbines. The assessment follows the method set out in [15], and the coefficient of power is calculated using Equation 2. The coefficient of power is averaged between the cut in speed (1 m/s) and rated power (3 m/s) to obtain a simple indication of turbine performance. All 'water-to-wire' losses up to the export terminals of the generator are included in the calculation. The assessment does not include electrical losses in the cables to shore, power converters, transformers or cables to the grid connection point. The current best estimate of the average coefficient of power (averaged over the four turbines) is C_p=0.41. This is an 8% increase on the contractual coefficient of power (C_p=0.38) that is required for the turbines to meet their target performance. This preliminary result indicates that the turbines are performing well in response to the different turbulent onset flows that have been observed at the Meygen site.

VI. Conclusions

Turbine and bed mounted ADCP measurements are presented to provide a preliminary assessment of the onset flow conditions to the Meygen Phase 1A turbines. The key findings are:

- Flow speeds are greatest at the north of the site at the locations of T1 and T3.
- The difference between the average ebb flow direction at T2 and T3 is 11°. The difference between the average flood flow direction at T2 and T3 is 12°.
- The onset boundary layer profiles vary significantly depending on flow direction. At T2 higher shear was observed during ebb tides.
- Flow twist in the boundary layer of around 7° has been observed, with small variations depending on location.
- Streamwise turbulence intensity is greatest during ebb tides at T2 and T3. This is in line with findings in [10]. Differences in ebb and flood streamwise turbulence at peak flow have also been observed at Naru Strait in Japan and the East River in the USA.
- In general the levels of streamwise turbulence intensity at Meygen are similar in magnitude to those measured at Kobe Strait in Japan [19] and the East River in New York, USA [12].
- The sea bed is significantly more rough upstream of T2 and T3 during ebb tides. The trench-like features

TABLE VI
SUMMARY OF WAVE HEIGHT AND ZERO UP CROSSING PERIOD (MEAN AND RANGE) DURING AUGUST AT T2 AND T3, AND NOVEMBER AT T4.

Sensor	Period	Wave height				Zero up crossing period			
		Range		Mean		Range		Mean	
		Flood	Ebb	Flood	Ebb	Flood	Ebb	Flood	Ebb
ADCP2	03/08/17 - 30/08/17	1.27	1.64	0.35	0.52	5.39	7.28	8.10	8.92
ADCP3	03/08/17 - 30/08/17	2.19	2.17	0.55	0.61	11.48	6.45	6.94	7.68
ADCP4	15/10/17 - 12/12/17	4.89	4.07	0.99	1.13	8.39	6.78	9.09	9.60

orientated perpendicular to the flow are likely to shed eddies off their trailing edge, augmenting turbulence to a greater extent during ebb tides than during flood tides at the study locations.

- The difference in measured wave parameters show lower mean values of both wave height and zero up crossing period during the flood tide. In most cases waves propagated with the flood tide, and opposed the ebb tide. Orbital motion caused by these higher wave states are a likely contributing factor to the higher levels of turbulence intensity that have been observed during ebb tides.
- Preliminary turbine performance analysis shows the turbines are exceeding their expected performance, showing good response to the temporally and spatially varying turbulent onset flows at the Meygen site.

VII. FURTHER WORK

Work is ongoing to:

- Quantify bed generated turbulence vs. wave generated turbulence at all turbine locations. This includes analysis of the turbulence generated by waves following the tide and waves opposing the tide.
- Correlate turbine performance to specific turbulent inflow features such as streamwise turbulence intensity and length scales. Results from this work will inform the micro-siting of future turbine installations.

ACKNOWLEDGEMENTS

Charles Greenwood was supported by the EPSRC FloWTurb project during this work (grant ref. number EP/N021487/1).

The authors would like to acknowledge Roving Eye Enterprises and Rousay Engineering Services for their support during the ADCP deployments and recovery.

REFERENCES

[1] D.Taaffe, Meygen Tidal Energy Project Phase 1A - Progress Update, Presentation, All Energy conference, Glasgow, 5th May 2018.
[2] Atlantis Resources Ltd, Project Development and Operation - Meygen, [Online] Accessed https://www.atlantisresourcesltd.com/projects/meygen/ on 17/03/2018.
[3] Atlantis Resources Ltd, Project Development and Operation - Ness of Duncansby, [Online] Accessed https://www.atlantisresourcesltd.com/projects/duncansby/ on 17/03/2018.
[4] Atlantis Resources Ltd, Project Development and Operation - Brough Ness, [Online] Accessed https://www.atlantisresourcesltd.com/projects/brough-ness/ on 17/03/2018.
[5] Open Hydro, Brims Tidal Array Environmental Statement, 2016.
[6] DP Energy, Westray South Tidal Array – Orkney, [Online] http://www.dpenergy.com/projects/tidal/westray-south/ on 17/03/2018.
[7] Scotrenewables, Lashy Sound, [Online] Accessed: http://www.scotrenewables.com/projects/lashy-sound on 17/03/2018.
[8] The European Marine Energy Centre (EMEC), Grid-connected tidal test site, [Online] Accessed: http://www.emec.org.uk/facilities/tidal-test-site/ on 17/03/2018.
[9] OFGEM, Typical Domestic Consumption Values, [Online] Accessed: https://www.ofgem.gov.uk/gas/retail-market/monitoring-data-and-statistics/typical-domestic-consumption-values on 17/03/2018.
[10] J.Hardwick, Field Characterisation of Currents and Near Surface Eddies in the Pentland Firth, Proceedings of the 4th Oxford Tidal Energy Workshop, 2015.
[11] I.Milne, Characteristics of the turbulence in the flow at a tidal stream power site, Philos. Trans. A. Math. Phys. Eng. Sci. 371:, 2012.
[12] I.Milne, The characterisation of the hydrodynamic loads on tidal turbines due to turbulence, Renewable and Sustainable Energy Reviews, 56:851-864, 2016
[13] J.Thomson, Measurements of turbulence at two tidal energy sites in Puget Sound, WA, IEEE Journal of Oceanic Engineering, 37(3):363-374, 2012.
[14] A.Bouferrouk, Quantifying turbulence from field measurements at a mixed low tidal energy site, Renewable Energy, 87:478-492, 2016.
[15] BSI, Marine energy – Wave, tidal and other water current converters, Part 200: Electricity producing tidal energy converters — Power performance assessment, London: The British Standards Institution. PD IEC/TS 62600-200:2013, 2013.
[16] B.Sellar, ReDAPT MD3.4 Interim Report: Turbulence Measurement and Characterisation, Report, Revision 1, 2012.
[17] M.Gilcotto, Robust Estimations of Current Velocities with Four-Beam Broadband ADCPs, Journal of Atmospheric and Oceanic Technology, 26: 2642-2654, 2009.
[18] D.Lande-Sudall, Co-located offshore wind and tidal stream turbines: Assessment of the energy yield and loading, Renewable Energy, 118: 627-643, 2018.
[19] P.Novo, Estimation of Tidal Peak Velocity by an Empirical Approach, Proceedings of the 12th European Wave and Tidal Energy Conference, 807-1-10, Cork, Ireland, 2017.
[20] J.Cui, Large-eddy simulation of turbulent flow in a channel with rib roughness, International Journal of Heat and Fluid Flow, 24(3): 372–388, 2003.
[21] A.Perry, Rough wall turbulent boundary layers, Journal of Fluid Mechanics, 37(2):383–413, 1969.
[22] L.Holthuijsen, Waves in Oceanic and Coastal Waters, Cambridge University Press, 2007.